



Structural model and capacity determination of underground reservoir in goaf: a case study of Shendong mining area in China

Zhijie Wen · Pengfei Jiang · Zhenqi Song ·
Yujing Jiang · Jinhao Wen · Suolin Jing

Received: 30 June 2023 / Accepted: 11 October 2023
© The Author(s) 2023

Abstract The large-scale extraction of coal resources in the western mining areas of China has resulted in a significant loss of water resources, which is a challenge for coordinating resource extraction with ecological preservation in the mining areas. Although underground reservoir technology can effectively solve this problem, measuring the storage capacity of underground reservoirs through engineering experiments is costly and time-consuming. Currently, there is a lack of accurate, reliable, and low-cost theoretical calculation solutions, which greatly restricts the promotion and application of underground reservoir technology. The theoretical calculation methods for underground reservoir capacity were

studied based on parameters from the Shendong mining area in China. A water storage structure model for coal mine underground water reservoirs was established, taking into account the settlement boundaries of the bedrock and loose layers in shallow coal seams, based on the key layer theory and the spatial structure model of the mining roof. The mathematical expression for the load on the coal-rock mass in the goaf was derived considering the rock breaking characteristics of the mining roof. The model determined the range of each water storage area, including the zone of loose body, zone of gradual load, and the compacted zone, based on the strength of the water storage capacity. The key parameters for calculating the water storage capacity were determined using a modified model for shallow thick loose layers and thin bedrock movement. Finally, a calculation method for the storage capacity was obtained. Based on the real data from the 22,615 working face of a mine in the Shendong mining area, the water storage capacity of the underground reservoir in the goaf was jointly calculated using FLAC^{3D}, Surfer 12.0 and the proposed calculation method. The calculated water storage capacity was approximately 1.0191 million m³. Although this result was 2.20% smaller than the on-site water pumping experiment data, it still verifies the feasibility of the above calculation method for determining the water storage capacity of underground water reservoirs.

Z. Wen · P. Jiang · Z. Song · Y. Jiang · S. Jing
College of Energy and Mining Engineering, Shandong
University of Science and Technology, Qingdao 266590,
Shandong, China

Z. Wen
Mining College, Guizhou University, Guiyang 550025,
Guizhou, China

Y. Jiang
Engineering Research Department, Nagasaki University,
Nagasaki 852-8521, Japan

J. Wen (✉)
School of Civil Engineering, Qingdao University
of Technology, Qingdao 266520, Shandong, China
e-mail: wenjh0532@163.com

Article highlights

- Based on the rock breaking characteristics of the overlying strata, a mathematical expression for the load on the coal-rock mass in the goaf was derived, and a 3D model of deformation of collapsed rocks in goaf under load was established.
- Based on the characteristics of surface subsidence and the 3D model of deformation of collapsed rocks in goaf under load, a water storage structure model for underground reservoirs in coal mines was established.
- A calculation method for the storage capacity of underground reservoirs, which is based on the volume of surface subsidence, was proposed.

Keywords Underground reservoir · Structural model · Water storage's capacity · Goaf · Shallow coal seam

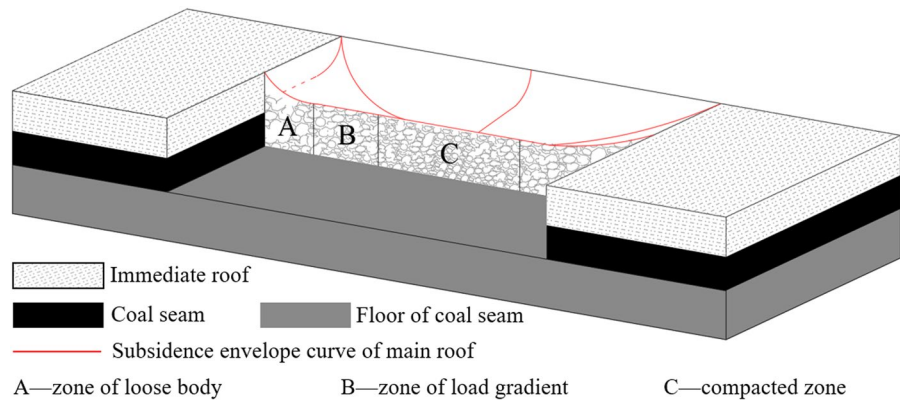
1 Introduction

The strategic focus of China's coal resources mining has gradually shifted westward, and the western mining area has become China's super large coal mining base. Owing to the large-scale exploitation of coal resources, the fragile ecological environment in the western mining area of China has further deteriorated, especially the massive loss of water resources, which seriously threatened the normal production and life in the mining area (Fan et al. 2020). To solve this contradiction, numerous studies have been conducted on water protection mining (Chi et al. 2019; Zhang et al. 2018). In addition to the water protection mining method, the research team led by Academician Gu (2015, 2021) proposes the coal mine underground reservoir technology, which effectively solved the problem of coordinated development of resource exploitation and ecological protection in mining areas. The underground coal mine reservoir utilizes overburden fractures caused by mining to direct water from the aquifer into the goaf, creating a sealed water storage area. This is achieved by connecting the coal pillar dam with an artificial dam at the goaf boundary, allowing for the storage and utilization of mine water (Kong et al. 2021; Menendez et al. 2019). However, in the process of underground reservoir operation,

the water stored in the reservoir will exert a force on the dam body, and floor of the underground reservoir, which was very easy to induce the dam body instability (Wang et al. 2019; Ordonez et al. 2012; Yao et al. 2019), bedplate seepage, etc. (Wen et al. 2021; Liu et al. 2019). These will affect the safe operation of underground reservoirs. Water effects on the dam body and floor of underground reservoir was related to the water storage volume. Therefore, it was of great significance to determine the reasonable water storage volume for the safe and efficient operation of underground reservoirs.

Coal mine underground reservoir is a construction mode that uses the remaining space after coal mining to protect water resources and improve the utilization rate of mine water conservancy (Shi 2021). Water storage volume is an important index to evaluate the operation efficiency of underground reservoirs, and there are many factors affecting the storage capacity (Du 2010; Jiang et al. 2022; Li et al. 2017). Cheng et al. (2016) believed that the water storage coefficient of coal mine underground reservoir is equal to the porosity of caving zone or fracture zone, and gives the calculation model of water storage volume of underground reservoir; Wang et al. (2018) studied the distribution law of stress and crushing expansion coefficient of collapsed rock mass in goaf through similar simulation tests, and obtained the relationship between stress and crushing expansion coefficient of water-saturated rock, which provided a theoretical basis for the prediction of water storage capacity and surface subsidence of coal mine underground reservoir; Ju et al. (2017) established the mathematical expression for water storage capacity of underground reservoir according to the different positions of the water storage level in the overburden collapse-fracture zone, and formed a determination method for determining the limit water storage volume and reasonable water storage volume of underground reservoirs; Fang et al. (2019) considered the potential influencing factors of water storage coefficient of coal mine underground reservoir comprehensively, established the mathematical model of water storage coefficient of underground reservoir under the influence of effective stress, and determined the analytical solution of the model. Many scholars have made great contributions to the calculation of water storage volume of underground reservoirs in coal mines. It is generally believed that the water storage area of underground

Fig. 1 Distribution map of Collapsed rock in goaf without accurate zoning



reservoir in coal mines is the free space in the collapsed rock and its upper fractured rock stratum in the goaf. However, the goaf is heterogeneous and porous media. After mining, the goaf is affected by the self-loading of overlying strata, and the void ratio gradually decreases until it tends to be stable (Wang et al. 2021). The change of the void ratio of coal and rock in the goaf can easily form invalid water storage space, which affects the spatial and temporal distribution of water body in goaf, so it is difficult to accurately determine the effective water storage volume of underground reservoir.

Taking into consideration these factors, when calculating the water storage space in underground reservoir area, this paper took the free water storage space as the benchmark, comprehensively considered the factors such as overburden fracture boundary and load distribution law, constructed the water storage structure model of the underground reservoir area, and reasonably determined the distribution range of effective water storage space in the goaf. Combining with the surface subsidence, it carried out the research on the calculation method of underground reservoir water storage volume.

2 Analysis of key parameters about the structural model

The water in the goaf is distributed in the coal and rock voids, and flows between the connected voids, which is the main structure for water storage in the underground reservoir. The compacted part of goaf is the key factor affecting the water storage volume in goaf. According to the existing research (Li et al.

2008), the goaf was roughly divided into the zone of loose body, zone of gradual load, and the compacted zone along the advancing direction of the working face (Fig. 1), and the accurate calculation of each sub-area has not been realized yet.

2.1 Analysis of load on rock in goaf

According to the failure boundary of thin bedrock, the damaged area from the roof of the working face to the top boundary of the overlying bedrock was approximately inverted funnel, while the damaged area from the top boundary of bedrock to the loose layer on the surface was approximately positive funnel. In order to calculate the load exerted by the overburden on the goaf, the model was simplified (Fig. 2). Taking the bottom boundary of the loose accumulation layer and the two vertices of the Conjugate analogous hyperbola (Zuo et al. 2017) as the boundary, it was approximately considered that its load acts directly on the broken bedrock and transmits the load to the collapsed rock mass in the goaf. The failure boundary of bedrock above the working face was Conjugate analogous hyperbola, and the dead weight load of the bedrock acts directly on the collapsed rock in the goaf.

The goaf was covered by broken bedrock and loose accumulation layer, and the load acting on the collapsed rock in the goaf was the superposition of the two loads. According to the model of the damaged boundary of bedrock with thick loose layer by Zuo et al. (2017), the following could be obtained:

$$a = \frac{1}{2} \left(L - \sum_{j=1}^m \cot \theta_{1j} h_j - \sum_{j=1}^m \cot \theta_{2j} h_j \right) \tag{1}$$

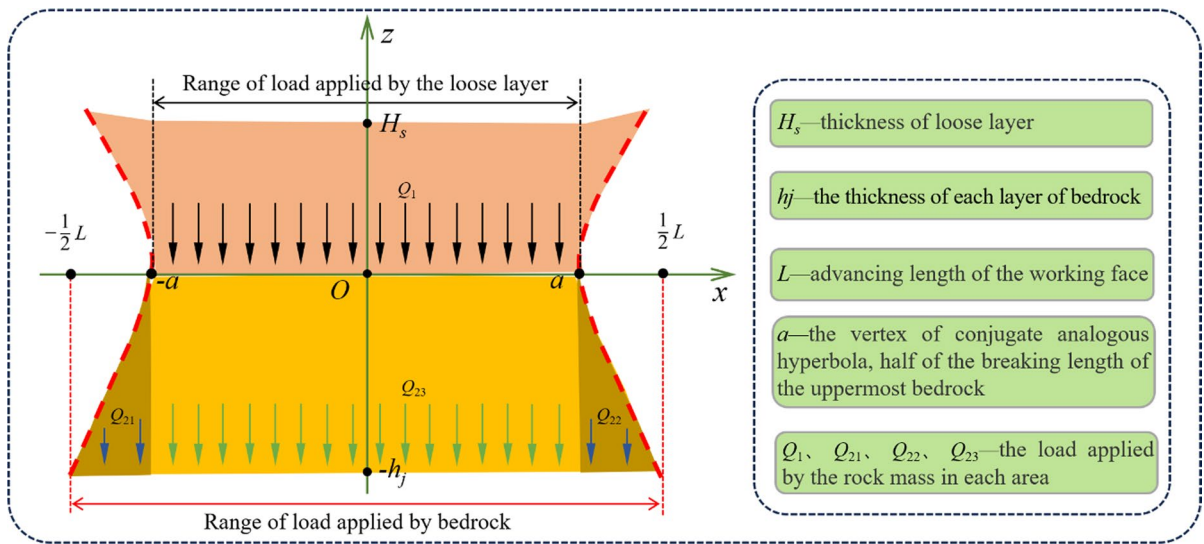


Fig. 2 Vertical load on the collapsed rock in the goaf (along the advancing direction)

where a is the vertex of Conjugate analogous hyperbola, half of the breaking length of the uppermost bedrock, m ; L is the advancing length of the working face, m ; m is the total number of strata in bedrock; h_j is the thickness of each layer of bedrock, m ; θ_{1j} , θ_{2j} is the initial collapse angle and periodic collapse angle of different strata in the bedrock, $^\circ$.

According to the known distance between the two vertices of Conjugate analogous hyperbola, combined with the thickness and average unit weight of the loose layer, the dead weight load (Q_1) of the loose layer acting indirectly on the collapsed rock in the goaf along the advancing direction of the working face can be obtained:

$$Q_1 = \gamma_s H_s \tag{2}$$

where Q_1 is the dead weight load of the loose layer acting indirectly on the collapsed rock mass in the goaf along the advancing direction of the working face, Pa ; γ_s is the volumetric weight of loose layer, N/m^3 ; H_s is the thickness of loose layer, m .

The direct load of bedrock broken at both ends in the advancing direction of the working face acting on the collapsed rock mass in the goaf was related to the initial collapse angle or periodic collapse angle of each rock stratum, and the Conjugate analogous hyperbola can approximately express its fracture boundary. According to the equation of

Conjugate analogous hyperbola model, the loads in the range of $(-1/2L, -a)$ and $(a, 1/2L)$ along the X axis are Q_{21} and Q_{22} respectively. The load of the bedrock above the goaf acting on the first layer of rock within the range of $(-1/2L, -a)$ along the X axis was:

$$\begin{aligned} Q_{21} &= \gamma_2 h_2 + \gamma_3 h_3 + \dots + \gamma_i h_i, \\ &- a \sqrt{1 + \frac{\left(\sum_{j=i}^m h_j\right)}{b^2}} \\ &\leq x < -a \sqrt{1 + \frac{\left(\sum_{j=i+1}^m h_j\right)}{b^2}} \end{aligned} \tag{3}$$

where a is the vertex of Conjugate analogous hyperbola, half of the breaking length of the uppermost bedrock, m ; γ_i is the unit weight of i -stratum, N/m^3 ; h_i is the thickness of i -stratum, m ; m is the total layers number of rock strata in bedrock; b is the semi imaginary axis length in the equation of Conjugate analogous hyperbola model, m .

$$b = a H_s \times \sqrt{1 / \left[\left(\int_0^{H_s} \cot(45^\circ + \varphi/2) L H_s + a \right)^2 - a^2 \right]} \tag{4}$$

where L is the advancing length of the working face, m ; H_s is the thickness of thick loose accumulation

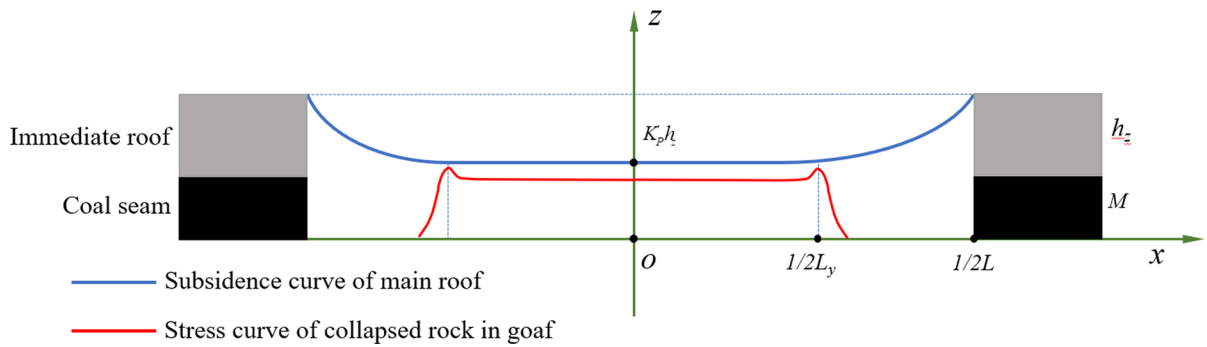


Fig. 3 Subsidence curve of main roof (along the advancing direction of working face)

layer, m ; φ is the internal friction angle of thick loose accumulation layer, $^\circ$.

Similarly, it can be seen that the load of overlying bedrock acting on the first layer in the range of $(a, 1/2L)$ along the X axis is:

$$Q_{22} = \gamma_2 h_2 + \dots + \gamma_i h_i, \quad a\sqrt{1 + \frac{(\sum_{j=i+1}^m h_j)^2}{b^2}} \leq x < a\sqrt{1 + \frac{(\sum_{j=i}^m h_j)^2}{b^2}} \quad (5)$$

The load of the overlying bedrock within the range of $(-a, a)$ along the X axis acting on the first layer of rock (main roof) was Q_{23} , and its load was the dead weight load of the overlying broken bedrock within this range:

$$Q_{23} = \gamma_2 h_2 + \gamma_3 h_3 + \dots + \gamma_i h_i + \dots + \gamma_m h_m \quad (6)$$

Combined with the load of the thick loose accumulation layer of subsidence, the mathematical expression of the superimposed load on the first stratum of the coal seam roof fracture is as follows:

$$Q = \begin{cases} \gamma_2 h_2 + \gamma_3 h_3 + \dots + \gamma_i h_i, & -a\sqrt{1 + \frac{(\sum_{j=i}^m h_j)^2}{b^2}} \leq x < -a\sqrt{1 + \frac{(\sum_{j=i+1}^m h_j)^2}{b^2}} \\ \gamma_s H_s + \gamma_2 h_2 + \gamma_3 h_3 + \dots + \gamma_i h_i + \dots + \gamma_m h_m, & -a \leq x < a \\ \gamma_2 h_2 + \gamma_3 h_3 + \dots + \gamma_i h_i, & a\sqrt{1 + \frac{(\sum_{j=i+1}^m h_j)^2}{b^2}} \leq x < a\sqrt{1 + \frac{(\sum_{j=i}^m h_j)^2}{b^2}} \end{cases} \quad (7)$$

2.2 Determination of the range of effective void zone

According to the load analysis of the loose layer and bedrock above the goaf, the load of the bedrock and loose layer that lose stability due to mining on the col-

lapsed rock in the goaf is unevenly distributed along the advancing direction of the working face or perpendicular to the advancing side, which was specifically manifested as: the load was low around the goaf and high in the middle of the goaf, and its value tended to be stable within a certain range (Fig. 3). The load difference of the collapsed rock in the goaf leads to the formation of three types of areas in the dip direction of the collapsed rock (the zone of loose body, zone of gradual load, and the compacted zone). The larger the void ratio between the collapsed rocks, the higher the water circulation and

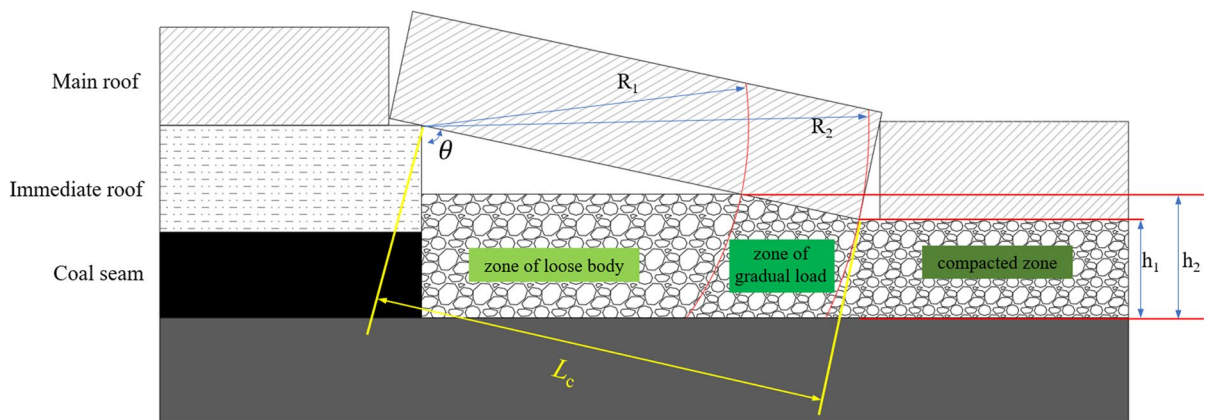


Fig. 4 Zoning map of collapsed rock in goaf after loading

water storage coefficient in the goaf. Therefore, the scientific division of the three types in the goaf is the basis for the effective calculation of the water storage volume of the underground reservoir.

Through existing studies, we can understand how the rock stratum breaks when the work was advancing forward: the rock stratum rotates and sinks with the coal wall as the fulcrum and half of the initial incoming pressure step (or periodic incoming pressure step) as the radius, which causes the collapsed rock to be affected by the load in the goaf while the adjacent fully subsided rock stratum acts on the collapsed rocks in the goaf to form the compacted zone (Fig. 4).

According to the geometric relationship in Fig. 4, the radius of loose accumulation zone was:

$$R_1 = \frac{L_c [M_c + (1 - K_p)h_z]}{M_c + (1 - K_p')h_z} \quad (8)$$

where L_c is the fracture length of rock beam above working face, m; K_p' is the residual expansion coefficient of collapsed rock in goaf; K_p is the initial coefficient of bulk increase of collapsed rock in goaf; M_c is the mining height of coal seam, m; h_z is the thickness of immediate roof, m.

According to the distribution law of the overburden load and the loaded zoning of the collapsed rock in the goaf, the three-dimensional spatial model bearing deformation of the collapsed rock in the goaf is reconstructed (Fig. 5), which realized the accurate division of the scope of the zone of loose body, zone of gradual load, and the compacted zone, in which the loose accumulation zone

was within the range from R_1 to the adjacent coal wall, the zone affected by the load was in the radius of R_1 and R_2 , while the stable compaction zone was near the middle of goaf.

2.3 Determination of the residual expansion coefficient

The range of effective voids can provide the basis for the calculation of water storage volume in goaf, and the residual expansion coefficient was the key parameter to determine the range of effective voids in goaf. Due to the shallow burial of coal seams in Western mining area, there was a corresponding relationship between the residual expansion coefficient and surface movement in physical space without considering the compression characteristics of the loose accumulation layer when it subsided.

The migration of the ground surface included the overall movement of the lower bedrock and the upper loose layer. As early as the 1950s, the Polish scholar Litvinisszyn (Tan 2020) introduced the random medium theory into study of surface subsidence, and then developed into probability integral method, which was widely used in the prediction of surface deformation and subsidence of mine engineering (Fig. 6).

Set the burial depth of the coal seam as h and the mining thickness of the coal seam as M_c . For a section of coal seam with a horizontal distance of s from the origin O and a mining length of ds in the coal seam, the smaller subsidence basin formed

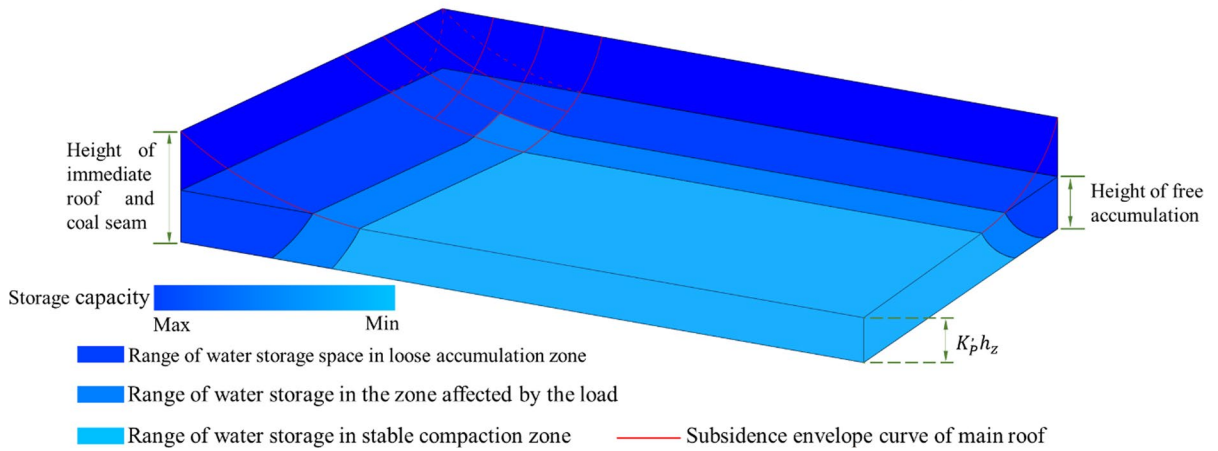


Fig. 5 The 3D model of deformation of collapsed rocks in goaf under load

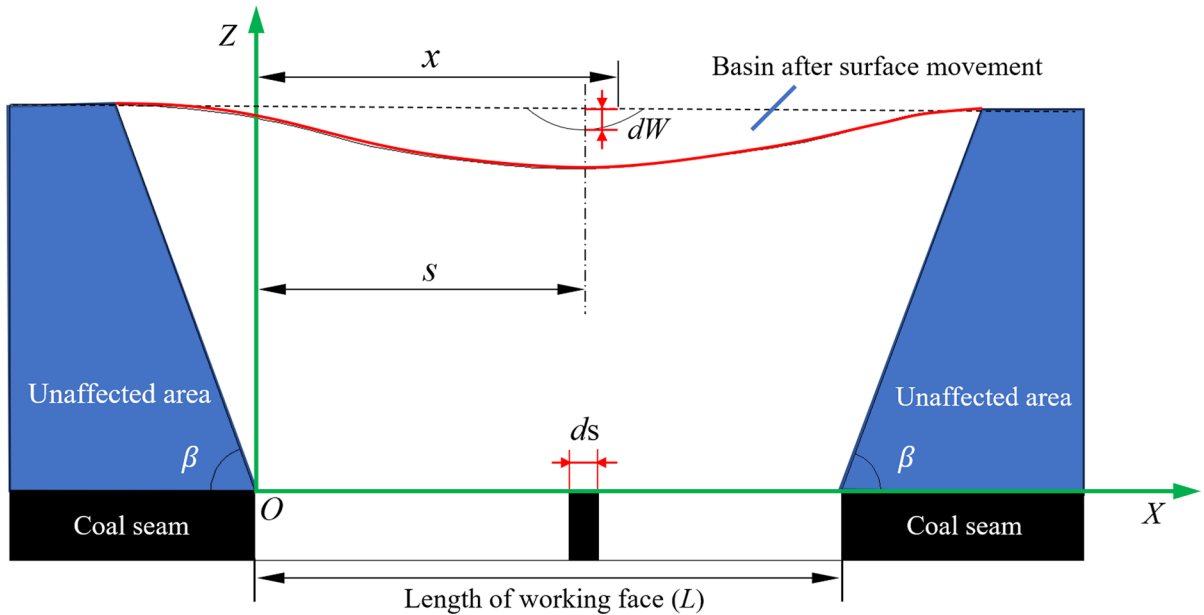


Fig. 6 Failure model of thick loose layer

at the position Z above it was dW , and its function expression was:

$$dW = qM_c \frac{h}{\sqrt{\pi}} e^{-h^2(x-s)^2} ds \tag{9}$$

According to the superposition principle, when the mining length was a random length (L), then:

$$W(x) = qM_c \frac{h}{\sqrt{\pi}} \int_0^L e^{-h^2(x-s)^2} ds \tag{10}$$

After further simplification:

$$W(x) = \frac{W_{cm}}{2} \left[\operatorname{erf} \left(\frac{\sqrt{\pi} x}{r} \right) + 1 \right] \tag{11}$$

where r is the main influence radius, m; W_{cm} is the maximum subsidence value of the surface, m; M_c is the mining thickness of the coal seam, m; $erf(x)$ is the solution value of the error integral table; q is the coefficient of subsidence; L is the mining length, m.

Different from the traditional funnel-shaped broken boundary model, this paper modifies the functional expression of settlement calculation based on the Conjugate analogous hyperbola model of thin bedrock with thick loose layer. Taking the failure vertex of the bedrock as the origin (O), the thickness of the loose layer was used to replace the buried depth of the coal seam. During the long-term water storage operation of the underground reservoir in the coal mine, the uncontrolled bedrock and loose layer above in the upper part of the goaf gradually tend to be stable. Especially for the thin bedrock with thick loose layer, due to the small number and thin thickness of the rock layer, the horizontal cracks and separation space generated by its fracture were gradually closed under the action of its dead load and loose layer load. The loose layer had good continuity, and the horizontal separation space and fracture space were small. Therefore, under the condition that the surface subsidence was basically stable and the compression deformation was not considered, there could be a spatial correspondence between the subsidence value and the residual expansion coefficient of the collapsed rock in the goaf (Fig. 7).

Its functional relationship was:

$$W_{cm} = M_c + h_z(1 - K_p') \quad (12)$$

The residual expansion coefficient of the collapsed rock in the goaf was:

$$K_p' = 1 - \frac{W_{cm} - M_c}{h_z} \quad (13)$$

3 Structural model of underground reservoir with overlying strata failure

In western China, Jurassic continental coal measures are the main mining areas. The coal seams are shallow and thick. The roof of the coal seams is sandstone generally, and the upper part of the bedrock is covered by thick quaternary eolian sand. The bedrock is shallow in the mining area, the rock strength is low and relatively developed fissures in the section greatly affected by surface water and weathering. The water storage volume is the free space between the collapsed coal and rock in the goaf. The distribution of the free space depends on the position and state characteristics of the rock above the working face. Researchers had conducted in-depth research on the movement and fracture law of rock strata above the working face for a long time, and further put forward

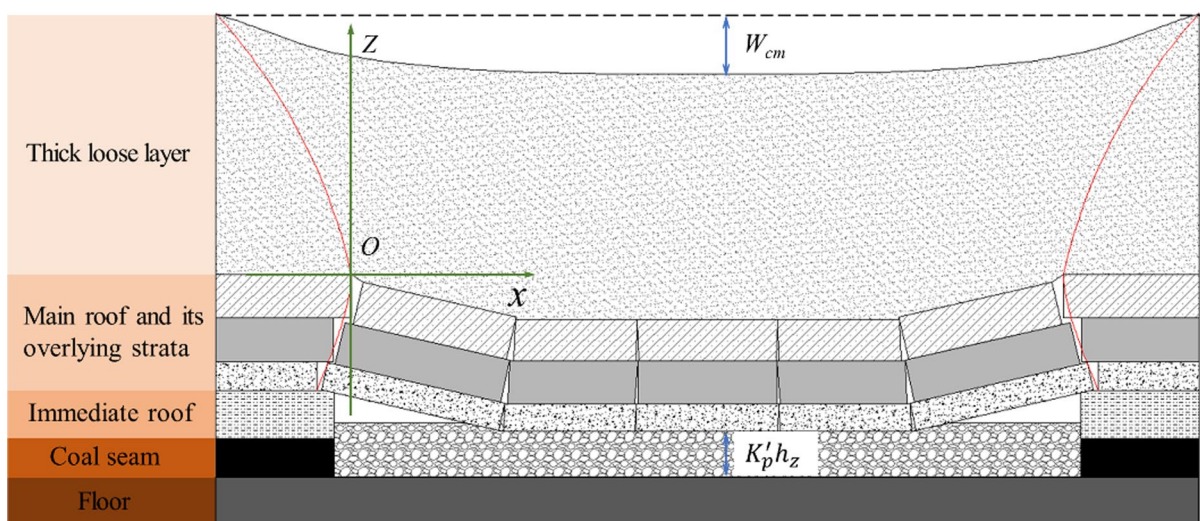


Fig. 7 Failure model of thin bedrock with thick loose layer

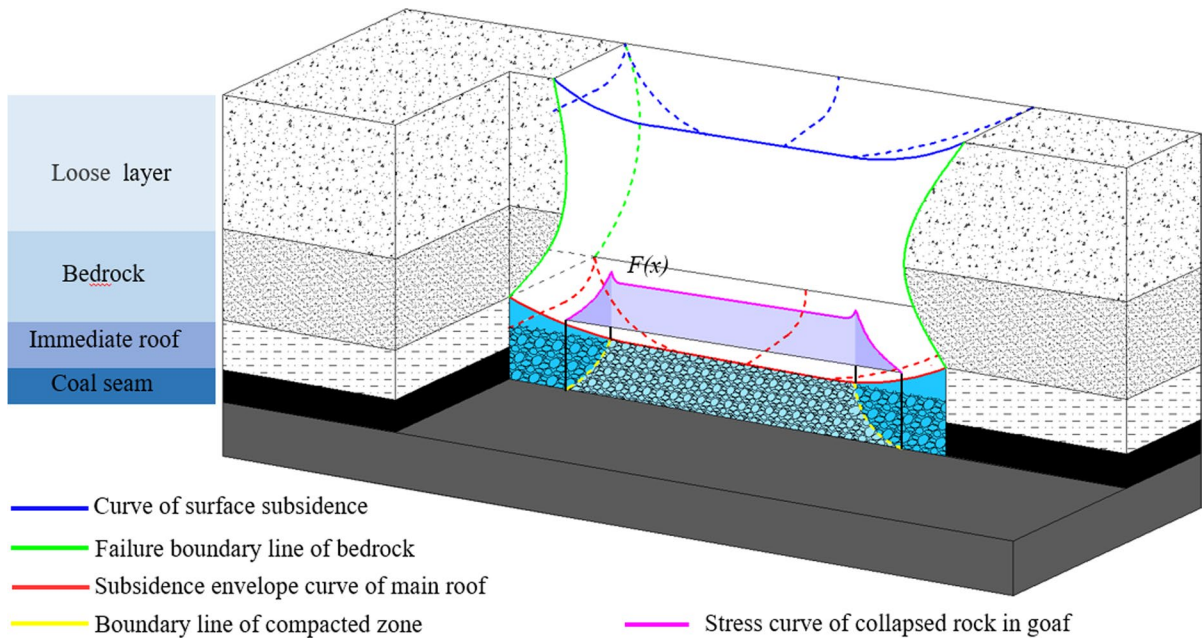


Fig. 8 Mechanical model of underground reservoir in coal mine

the key strata theory of rock formation control based on the “Voussoir Beam” theory (Sun et al. 2019). When the overlying strata on the stope are fully affected by mining, the rupture of key strata leads to surface subsidence, forming a collapsed basin. The geometric boundary of collapse basin is related to the thickness of loose layer and bedrock. The thicker the loose layer and the thinner the bedrock, the larger the scope of collapse basin formed. According to the failure model of thin bedrock with thick loose layer, the 3D model of deformation of collapsed rocks in goaf under load, stress curve of collapsed rock in goaf and the main roof settlement envelope, the structural model of underground reservoir could be established (Fig. 8). Its main water storage space is the free space in the goaf.

4 Calculation method of water storage capacity

With the data of surface subsidence and mining parameters, the water storage can be calculated according to the coal mining amount, surface subsidence amount and unused empty area volume of goaf.

$$V = V_K + V_Z - V_C - V_a - V_y \tag{14}$$

where V_K is the volume of coal mining space, m^3 ; V_Z is the volume of collapsed direct roof, m^3 ; V_C is the surface subsidence volume, m^3 ; V_y is the volume of invalid space in the compacted zone in the goaf, m^3 ; V_a is the solid’s volume of collapsed rock in the area outside the compacted zone, m^3 .

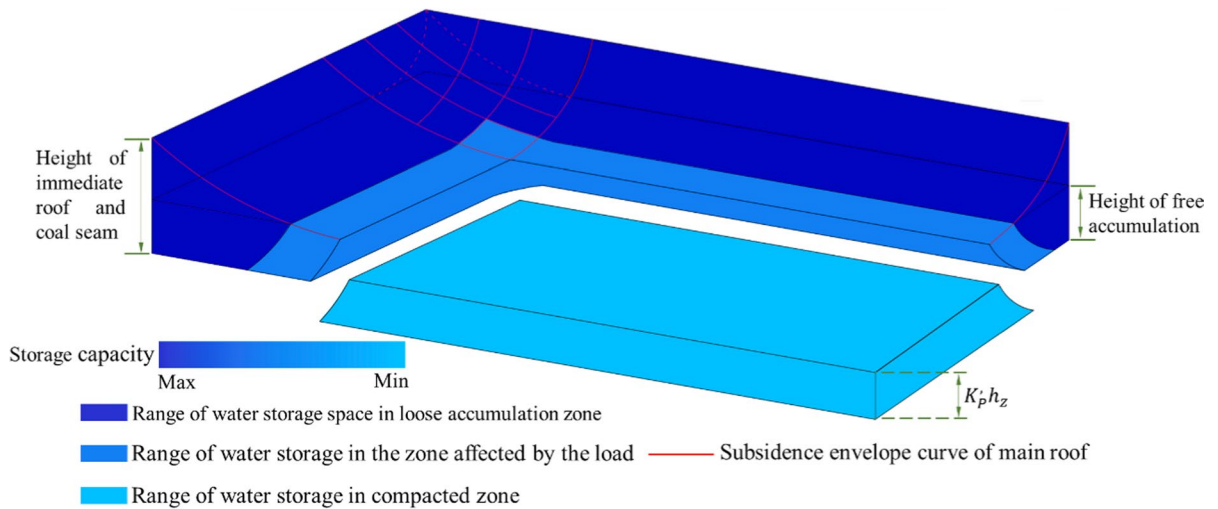
The space occupied by the collapsed rock in the loose accumulation zone and the zone affected by the load after collapse can be regarded as the volume of the unbroken solid (V_a) and a part of the void volume, while the volume of the stable compaction zone was the volume of the expansion of the rock after collapse ($K_p'V_b$), and the immediate roof of the collapse was composed of V_a and V_b :

$$V_Z = V_a + V_b \tag{15}$$

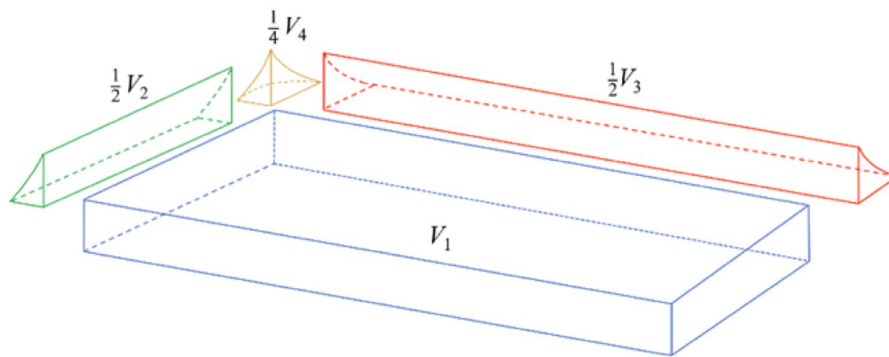
The solid’s volume of collapsed rock in the stable compacted area of goaf is V_b , and there were:

$$V_b = \frac{V_y}{K_p'} \tag{16}$$

Bring V_a and V_b into Eq. (14) and simplify them to get:



(a) Volume of compacted zone



(b) Split of compacted zone

Fig. 9 Schematic diagram of volume calculation of compacted zone

$$V = V_K - V_C + V_y \left(\frac{1}{K_p'} - 1 \right) \tag{17}$$

where V is the theoretical water storage volume of underground reservoir, m^3 ; K_p' is the residual expansion coefficient of collapsed rock in the compacted zone.

The solid's volume of coal mined in the working face (V_K) was:

$$V_K = L \times B \times M_C \tag{18}$$

where L is the advancing length of the working face, m; B is the width of working face, m; M_C is the mining height of coal seam, m.

The volume (V_y) of the compacted zone of the collapsed rock in the goaf can be further calculated according to the 3D model in Fig. 5. The volume of this part can be divided into four parts for separate calculation (Fig. 9).

$$V_y = V_1 + V_2 + V_3 + V_4 \tag{19}$$

$$B = \sqrt{L_B^2 - [M_C + h_z(1 - K_{p'})]^2} - \sqrt{L_B^2 - (z - M_C - h_z)^2} \tag{25}$$

$$V_1 = \left(L - 2\sqrt{L_c^2 - [M_C + h_z(1 - K_{p'})]^2} \right) \times \left(B - 2\sqrt{L_B^2 - [M_C + h_z(1 - K_{p'})]^2} \right) \times M_c \tag{20}$$

$$V_2 = 2 \left(B - \sqrt{L_B^2 - [M_C + h_z(1 - K_{p'})]^2} \right) \int_{\sqrt{L_c^2 - [M_C + h_z(1 - K_{p'})]^2}}^{\sqrt{L_c^2 - (M_C + h_z)^2}} \sqrt{L_c^2 - x^2} dx \tag{21}$$

$$V_3 = 2 \left(L - \sqrt{L_c^2 - [M_C + h_z(1 - K_{p'})]^2} \right) \int_{\sqrt{L_B^2 - [M_C + h_z(1 - K_{p'})]^2}}^{\sqrt{L_B^2 - (M_C + h_z)^2}} \sqrt{L_B^2 - x^2} dx \tag{22}$$

where L is the advancing length of the working face, m; L_c is the fracture length of rock beam fracture at the initial pressure along the advancing direction of the working face, m; B is the width of working face, m; L_B is the initial fracture length of rock beam perpendicular to the advancing direction of the working face, m; M_c is the mining thickness of the coal seam, m.

V_1 is the volume of the middle part of the stable compaction area, which can be regarded as a cuboid. V_2 is the envelope space formed by the compaction boundary line and the vertical plane at the open cut and stope line of the working face. V_3 is the envelope space formed by the boundary line and vertical plane of the compaction area on both sides of the advancing direction of the working face.

V_4 is a spatial envelope composed of an ellipse with $2\sqrt{L_c^2 - [M_C + h_z(1 - K_{p'})]^2}$ and $2\sqrt{L_B^2 - [M_C + h_z(1 - K_{p'})]^2}$ as the maximum major axis and the maximum minor axis respectively as the bottom surface and a function about x and y as the envelope. Integrate d_z within the range of $[0, M_c + h_z]$ to obtain:

$$V_4 = 4\pi \int_0^{M_c + h_z} AB dz \tag{23}$$

$$A = \sqrt{L_c^2 - [M_C + h_z(1 - K_{p'})]^2} - \sqrt{L_c^2 - (z - M_C - h_z)^2} \tag{24}$$

5 Case study




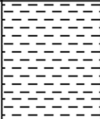


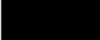
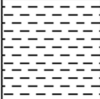

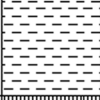

A coal mine was located on the Bank of Wulanmulun River in China. The surface of the mine field was widely covered with modern aeolian sand and Quaternary loess, and tmoukuhe main coal bearing stratum was the middle and lower Jurassic Yan'an formation (J1~2Y), which was widely distributed. The mine had carried out the construction of underground reservoir in the goaf of 22,615 working face of 2⁻² coal seam, which has been put into use at present. The average thickness of the coal seam was 5.15 m, and the design mining height was 4.5 m (Fig. 10). A goaf with a width of 350.6 m and a length of 1470.5 m was formed after the mining of the working face.

5.1 Numerical simulation of load and surface's displacement

5.1.1 Parameter selection and model design

The dimensions of the computational model were 2000 m×600 m×130 m, as illustrated in Fig. 11. Model boundary conditions are set as follows: the horizontal displacement of the front-back and right-left side faces, fixed; the bottom boundary fixed; the top surface, free. According to the mechanical characteristics of overburden strata, the constitutive relation

Fig. 10 General stratigraphic column

| Succession of strata | Diagram | Layer thickness (m) | | Rock character |
|----------------------|---|---------------------|--------------|--|
| | | Average value | Extremum | |
| 1 |  | 4.10 | 1.50 ~10.06 | Aeolian sand layer |
| 2 |  | 50.9 | 30.44 ~60.21 | Loess and clay |
| 3 |  | 3.00 | 0 ~7.40 | Coarse sandstone |
| 4 |  | 7.60 | 2.95 ~9.90 | It is mainly siltstone, and some areas are sandy mudstone, medium sandstone and coarse sandstone |
| 5 |  | 4.80 | 1.75 ~12.81 | It is mainly sandy mudstone, and some areas are siltstone |
| 6 |  | 0.15 | 0 ~0.44 | Mudstone with horizontal bedding |
| 7 |  | 5.10 | 4.73 ~5.55 | 2-2 coal seam |
| 8 |  | 11.04 | 7.02 ~14.81 | It is mainly siltstone, and some sections are mudstone or fine sandstone |
| 9 |  | 2.60 | 2.02 ~3.81 | Fine sandstone |
| 10 |  | 24.12 | 17.2 ~28.81 | It is mainly siltstone, and some sections are mudstone or fine sandstone |
| 11 |  | 16.05 | 10.2 ~19.65 | Fine sandstone |

of coal and rock mass were both Mohr–coulomb criteria. The initial velocities in both horizontal and vertical directions are set to 0. The finite elements, 840,000, and grid points 899,469, in total, were laid out based on the geometrical dimension of the model. The coal seam was mined at a rate of 20 m per step, with a total mining distance of 1470 m. Table 1 provides the specific physical and mechanical parameters for each rock stratum.

The cohesion force, friction angle, and tensile strength of contacts in FLAC^{3D} were calibrated through a series of uniaxial compression tests. The meshing of rock samples was consistent with the model. Additionally, the initial values of microscopic parameters were estimated based on material properties. Iterative calculations were then conducted until the uniaxial compressive strength and elastic modulus of the samples match the rock mass data in Table 1; the results are shown in Fig. 12. Because

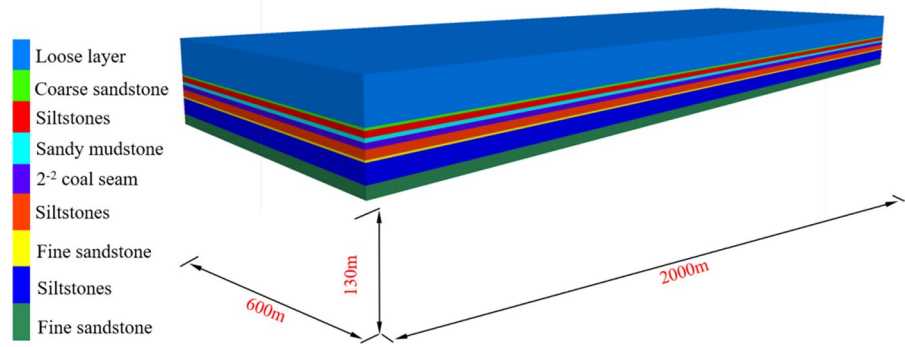
the calibration process is consistent, to highlight the research focus, only one layer of rock stratum calibration curve was listed.

Based on the geological conditions of working face 22,615 in a specific mine, the overlying strata failure was simulated by considering the ratio of maximum to minimum horizontal principal stresses and the ratio of maximum horizontal principal stress to vertical stress, with a mining thickness of 5.1 m. The model was subsequently calibrated with reference to existing research findings (Guo et al. 2020). Table 2 presented the parameters of the contact surfaces between each rock layer.

5.1.2 Analysis of results

The stress distribution of the stope after coal mining was shown in Fig. 13. The vertical bearing pressure in the goaf was symmetrically distributed along the

Fig. 11 Calculation model of numerical simulation of working face mining



central axis of the goaf, forming a stress concentration area higher than the initial stress in the coal rock mass around the goaf, and forming a bearing stress relief area less than the initial stress at the junction of the goaf and the coal rock mass near the goaf. The vertical support stress along or perpendicular to the advancing direction of the working face gradually increased and gradually returned to the initial stress state.

By analyzing the stress distribution characteristics, it was concluded that the loose accumulation zone was within 0–18 m from the open-off cut (or stopping line) along the advancing direction of the working face; The area about 18–25 m away from the open cut (or stopping line) was the load affected zone, and the rest was the compaction stability zone. Perpendicular to the advancing direction of the working face, the loose accumulation zone was within the range of about 0–14 m from the coal walls on both sides, the load affected zone was within the range of about 14–20 m from the coal walls on both sides, and the rest was the compaction stability zone.

2⁻²# coal belongs to shallow-buried coal seam, and the overlying bedrock is thin. During the mining of

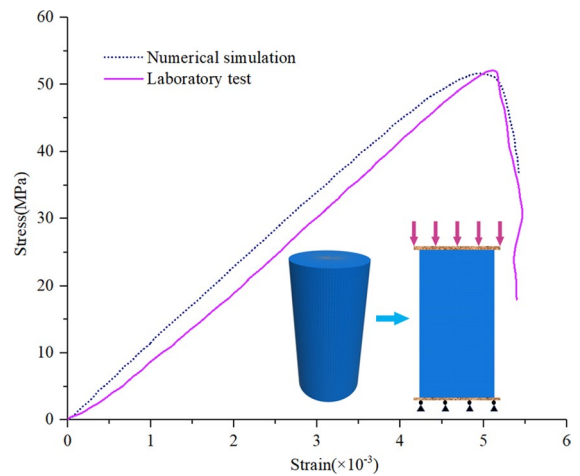


Fig. 12 Iterative calculation results

this coal seam, the main roof above the working face was broken for the first time, forming cracks directly to the surface, resulting in surface subsidence. Figure 14 showed the contour map of surface subsidence when the working face advances to 500 m, 1000 m and 1470 m respectively. With the advancing of the

Table 1 Physico-mechanical parameters of coal and rocks in Western Mining Area

| Rock character | Volumetric weight (kN m ⁻³) | Compressive strength (MPa) | Tensile strength (MPa) | Elastic modulus (GPa) | Cohesive forces (MPa) | The angle of internal friction (°) |
|---------------------------|---|----------------------------|------------------------|-----------------------|-----------------------|------------------------------------|
| Loose layer | 17.0 | 3.21 | 0.51 | 1.12 | 1.0 | 38.0 |
| Sandy mudstone | 24.6 | 51.9 | 3.18 | 10.31 | 6.8 | 38.0 |
| Siltstones | 24.5 | 66.6 | 3.37 | 13.22 | 7.1 | 38.3 |
| Fine sandstone | 24.1 | 63.9 | 3.66 | 13.21 | 6.5 | 38.5 |
| Gritstone | 23.4 | 43.2 | 3.13 | 13.91 | 4.4 | 42.0 |
| 2 ⁻² coal seam | 13.1 | 14.5 | 0.71 | 1.52 | 2.6 | 39.9 |

Table 2 Mechanical parameters of contact between rock layers

| / | k_n (GPa/m) | k_s (GPa/m) | c (MPa) | φ (°) |
|----------------------------|---------------|---------------|-----------|---------------|
| Loose layer-Sandy mudstone | 2.8 | 0.9 | 0.6 | 27.0 |
| Sandy mudstone-Siltstones | 20.1 | 8.4 | 1.7 | 28.0 |
| Siltstones-Fine sandstone | 27.5 | 10.1 | 1.9 | 22.4 |
| Fine sandstone-Gritstone | 26.2 | 9.2 | 1.8 | 21.2 |
| Gritstone-2-2 coal seam | 9.5 | 3.8 | 1.1 | 18.5 |

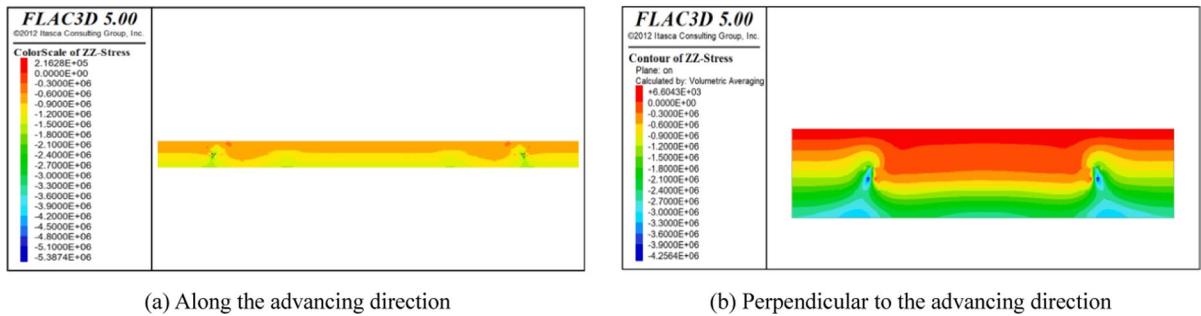


Fig. 13 Cloud diagram of vertical support stress in goaf with working face advancing to 1470 m

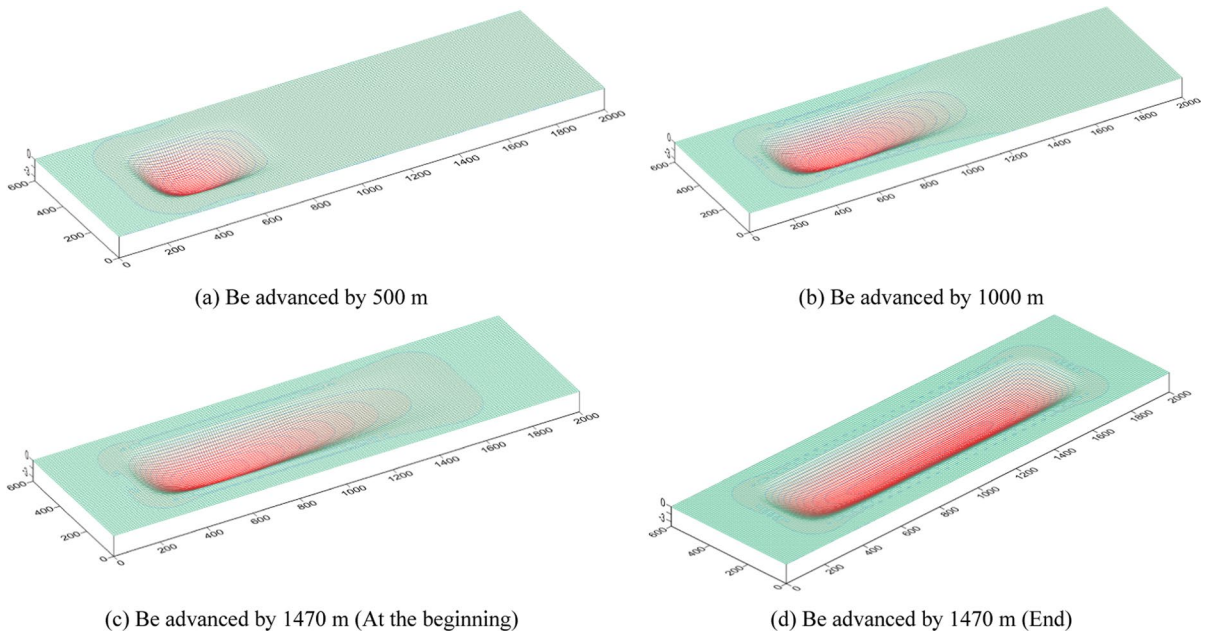


Fig. 14 Surface's subsidence contour during working face advancing

working face, the affected area of the surface gradually extends forward, and the subsidence value also increased, and finally a subsidence basin beyond the actual mining boundary of the working face was

formed. The numerical simulation results show that the maximum surface subsidence was 3.035 m. Referring to the relevant research on the surface subsidence of 22,615 working face in reference, 27 and 30

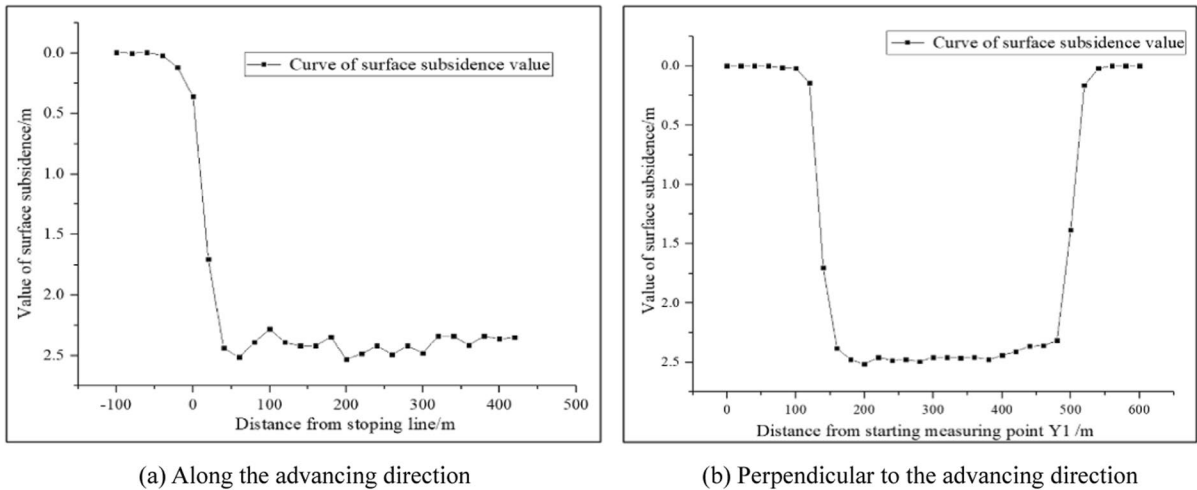


Fig. 15 Surface’s subsidence curve measured on site

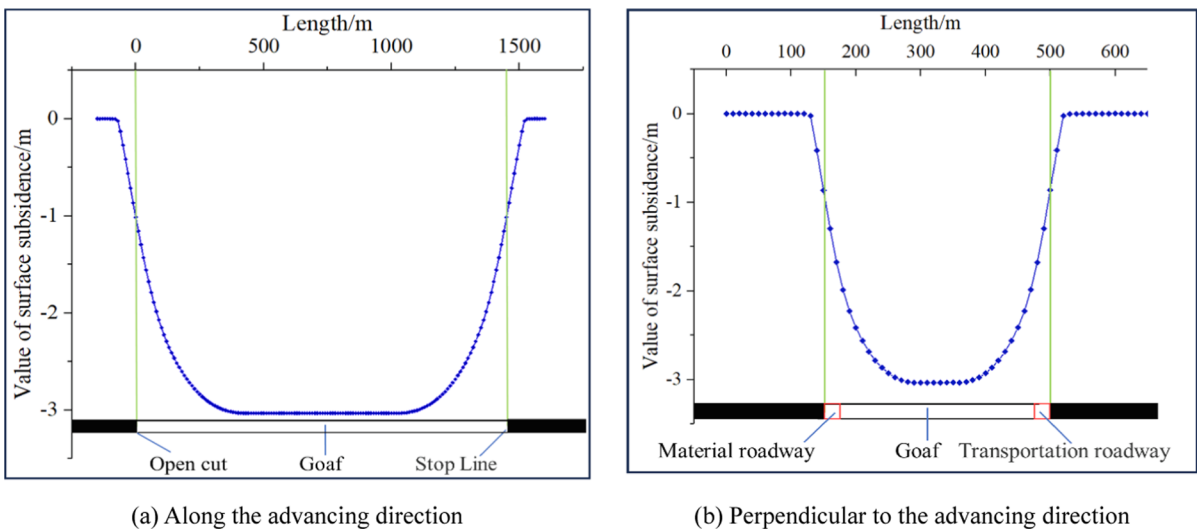


Fig. 16 Surface’s subsidence curve of 22,615 working face obtained by numerical simulation

measuring points were buried on the surface observation line along the advancing direction of the working face and perpendicular to the advancing direction, and the embedding spacing of all measuring points was 20 m (Wu 2017). The initial surface subsidence data measured on site was shown in Fig. 15, with the maximum surface subsidence value of 2.57 m, and the field observation data was 0.465 m smaller than the numerical simulation data (Fig. 16), the field observation and numerical simulation results fit well.

5.2 Calculation and verification of underground reservoir’s capacity

22,615 working face was covered with thick loose layer and thin bedrock, and the water storage volume was calculated according to the established structure model of underground reservoir. The coal extraction volume (V_K) calculated based on Eq. (18) and the parameters and monitoring data of the working face is determined to be 2,315,250

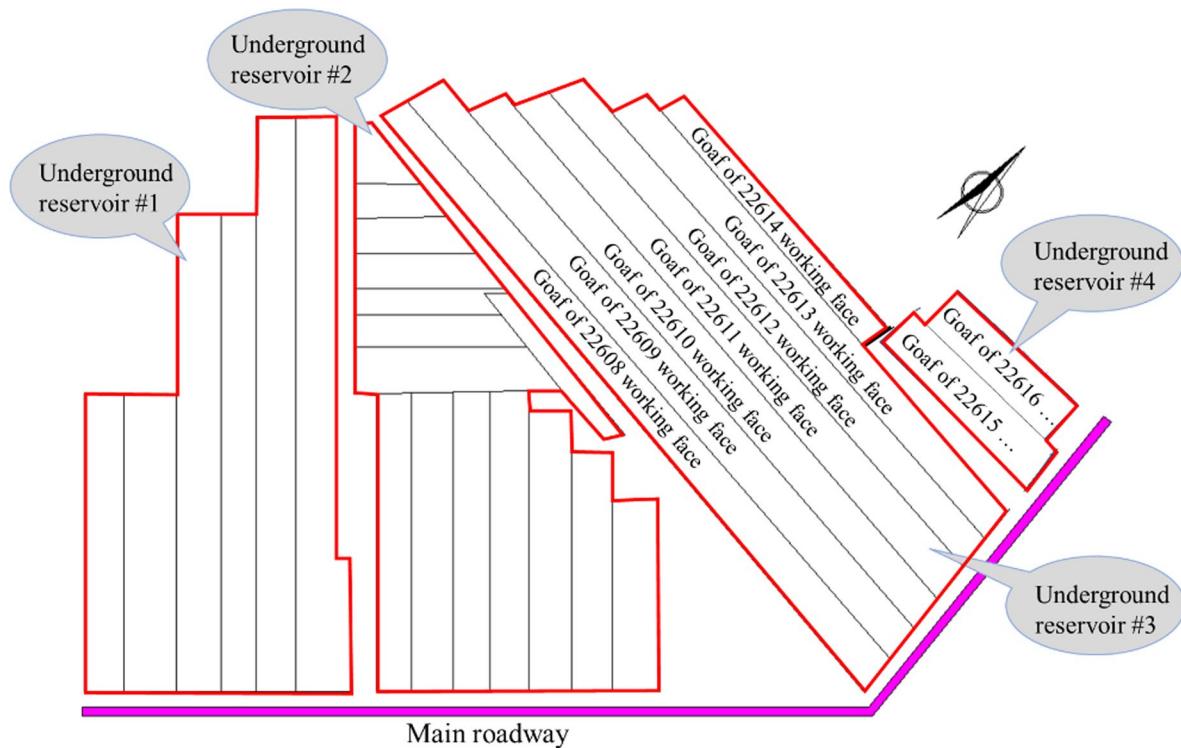


Fig. 17 Distribution plan of underground reservoir of a mine in Western mining area of China

m^3 . According to the numerical simulation results, the final settlement data of overburden pushed to 1470 m of the working face was selected as the calculation basis. The data was imported into Surfer 12.0, and the net volume of overburden subsidence was $1,144,392 \text{ m}^3$ by processing the built-in calculation command. The volume of the compacted zone in the goaf can be calculated according to the three-dimensional model of the pressure bearing deformation distribution range of the collapsed rock in the goaf. The volume of the compacted zone (V_y) in the goaf was $2,047,711 \text{ m}^3$ by bringing relevant parameters into Eqs. (19)–(25). Finally, the water storage volume (V) calculated by Eq. (17) was $1,019,176 \text{ m}^3$.

According to the field drainage water experiment data (Shi 2016), the water storage capacity of the goaf in 22,615 working face was about $104,2141 \text{ m}^3$ (Fig. 17). The results obtained in this paper were slightly 2.20% smaller than the field drainage experiment data, but the calculated results were within the reasonable range. It effectively solved the problems

of high cost and time-consuming in the field drainage test.

6 Conclusions

A water storage structure model of shallow coal seam underground reservoir in Western mining area of China was established. Based on the characteristics of surface's subsidence in stope, the mathematical formula of water storage volume in goaf was derived, and the calculation method of water storage capacity of underground reservoir was proposed.

The load on the coal and rock mass caving in the goaf had the characteristics of “low around and high in the middle”, which leads to the differential distribution of the compaction rate of the coal and rock mass caving in the goaf, which was very easy to form an invalid water storage space between the coal and rock mass in the middle of the goaf. The water storage space of the underground reservoir was mainly a free void space formed by mining disturbance, and

the invalid water storage space in compaction zone of goaf should be ignored when calculating the water storage volume.

According to the length of fractured rock, the zone of loose body was within the range from R_1 to the adjacent coal wall; the zone of gradual load was in the radius within the range of R_1 and R_2 was in the circle of radius; the compacted zone was near the middle of goaf. According to the distribution range of different areas, the pressure bearing deformation structure model of caving coal and rock mass in goaf was established, and the method of determining the residual fragmentation expansion coefficient of caving coal and rock mass in goaf through the surface's settlement value was proposed.

Through numerical simulation and theoretical calculation, the zone of loose body, the zone of gradual load and the compacted zone of falling gangue in the goaf of 22,615 working face along the strike and dip of the working face were obtained. Through numerical simulation, the maximum surface settlement was 4.047 m, and the net volume of subsidence was 114 4400 m³. On this basis, the water storage volume of 22,615 working face was about 101 9100 m³, which had a good fit with the field drainage results.

Author contribution ZW and YJ made substantial contributions to the conception or design of the work; PJ wrote the main manuscript text; ZS checked the manuscript and ensured article quality; JW and SJ guided the design and modification of the picture; All authors reviewed the manuscript.

Funding This work was supported by National Natural Science Foundation of China (51974174, 52274130, 52204140), and Shandong Excellent Youth Fund (ZR2019YQ26).

Data availability Data will be made available on request.

Declarations

Competing interests The authors declare no competing interests.

Ethics approval and consent to participate Not applicable.

Consent to publish The Authors confirm: that neither the manuscript nor any parts of its content are currently under consideration or published in another journal; that its publication has been approved by all co-authors; all of the material is owned by the authors and/or no permissions are required.

Competing interest The authors have no competing interests as defined by Springer, or other interests that might be perceived to influence the results and/or discussion reported in this paper.

Open Access This article is licensed under a Creative Commons Attribution 4.0 International License, which permits use, sharing, adaptation, distribution and reproduction in any medium or format, as long as you give appropriate credit to the original author(s) and the source, provide a link to the Creative Commons licence, and indicate if changes were made. The images or other third party material in this article are included in the article's Creative Commons licence, unless indicated otherwise in a credit line to the material. If material is not included in the article's Creative Commons licence and your intended use is not permitted by statutory regulation or exceeds the permitted use, you will need to obtain permission directly from the copyright holder. To view a copy of this licence, visit <http://creativecommons.org/licenses/by/4.0/>.

References

- Alvarez R, Ordonez A, Garcia R et al (2018) An estimation of water resources in flooded, connected underground mines. *Eng Geol* 232:114–122. <https://doi.org/10.1016/j.enggeo.2017.11.016>
- Chen SS (2016) Research on the key technology of water resources recycling utilization in the underground goaf reservoir in Shandong mining area. Ph.D, Dissertation, Xi'an University of Science and Technology, Xian, China
- Chi MB, Zhang DS, Liu HL et al (2019) Simulation analysis of water resource damage feature and development degree of mining-induced fracture at ecologically fragile mining area. *Environ Earth Sci* 78:88. <https://doi.org/10.1007/s12665-018-8039-5>
- Du SH (2010) An estimation of water resources in flooded, connected underground mines. *Yellow River* 32(02):64–65
- Fan JY, Xie HP, Jie C et al (2020) Preliminary feasibility analysis of a hybrid pumped-hydro energy storage system using abandoned coal mine goafs. *Appl Energy*. <https://doi.org/10.1016/j.apenergy.2019.114007>
- Fang J, Song HQ, Xu JJ et al (2019) Storage coefficient calculation model of coal mine underground reservoir considering effect of effective stress. *J China Coal Soc* 44(12):3750–3759. <https://doi.org/10.13225/j.cnki.jccs.SH19.1147>
- Gu DZ (2015) Theory framework and technological system of coal mine underground reservoir. *J China Coal Soc* 40(02):239–246. <https://doi.org/10.13225/j.cnki.jccs.2014.1661>
- Gu DZ, Li JF, Cao ZG et al (2021) Technology and engineering development strategy of water protection and utilization of coal mine in China. *J China Coal Soc* 46(10):3079–3089. <https://doi.org/10.13225/j.cnki.jccs.2021.0917>
- Guo WB, Zhao GB, Bai EH (2020) Critical failure of overlying rock strata and its criteria induced by high-intensity

- longwall mining. *J China Coal Soc* 45(11):3657–3666. <https://doi.org/10.13225/j.cnki.jccs.2019.1335>
- Jiang BB, Gao J, Du K et al (2022) Insight into the water–rock interaction process and purification mechanism of mine water in underground reservoir of Daliuta coal mine in China. *Environ Sci Pollut Res*. <https://doi.org/10.1007/s11356-021-18161-3>
- Ju JF, Xu JL, Zhu WB (2017) Storage capacity of underground reservoir in the Chinese western water-short coalfield. *J China Coal Soc* 42(02):381–387. <https://doi.org/10.13225/j.cnki.jccs.2016.6016>
- Kong XS, Xu ZZ, Shan RL et al (2021) Investigation on groove depth of artificial dam of underground reservoir in coal mines. *Environ Earth Sci* 80(06):214. <https://doi.org/10.1007/s12665-021-09520-x>
- Li QS, Ju JF, Cao ZG et al (2017) Suitability evaluation of underground reservoir technology based on the discriminant of the height of water conduction fracture zone. *J China Coal Soc* 42(08):2116–2124. <https://doi.org/10.13225/j.cnki.jccs.2016.1871>
- Li SG, Zhang W, Zou YX et al (2008) Numerical simulation of gas seepage law in fully mechanized top coal caving goaf [J]. *Min Saf Environ Prot* 35(2):1–3
- Liu XL, Cao ZG, Chen SS et al (2019) Seepage field analysis and optimal schedule of distributed underground reservoir in mining area. *J China Coal Soc* 44(12):3693–3699. <https://doi.org/10.13225/j.cnki.jccs.SH19.1167>
- Menendez J, Loredó J, Galdo M et al (2019) Energy storage in underground coal mines in NW Spain: assessment of an underground lower water reservoir and preliminary energy balance. *Renew Energy* 134:1381–1391. <https://doi.org/10.1016/j.renene.2018.09.042>
- Ordonez A, Jardon S, Alvarez R et al (2012) Hydrogeological definition and applicability of abandoned coal mines as water reservoirs. *J Environ Monit* 14(8):2127–2136. <https://doi.org/10.1039/C2EM11036A>
- Shi XC (2016) Study on deformation-failure of overlying strata induced by coal mining and its permeability assessment. Ph.D, Dissertation, China University of mining and Technology (Beijing), Beijing, China
- Shi XC (2021) Research progress and prospect of underground mines in coal mines. *Coal Sci Technol* 50:1–10
- Sun YJ, Zuo JP, Murat K et al (2019) A novel method for predicting movement and damage of overburden caused by shallow coal mining. *Rock Mech Rock Eng* 53(4):1545–1563. <https://doi.org/10.1007/s00603-019-01988-1>
- Tan XF, Song BZ, Bo HZ et al (2020) Extraction of irregularly shaped coal mining area induced ground subsidence prediction based on probability integral method. *Appl Sci Basel*. <https://doi.org/10.3390/app10186623>
- Wang BF, Liang B, Wang JG et al (2018) Experiment study on rock bulking of coal mine underground reservoir. *Rock Soil Mech* 39(11):4086–4092. <https://doi.org/10.16285/j.rsm.2017.0506>
- Wang FT, Liang NN, Li G et al (2019) Failure evolution mechanism of coal pillar dams in complex stress environment. *J Min Saf Eng* 36(06):1145–1152. <https://doi.org/10.13545/j.cnki.jmse.2019.06.010>
- Wang WN, Yao QL, Tang CJ et al (2021) Study of the mechanical properties and fracture evolution of sandstone with different moisture contents under true triaxial stress. *Arab J Sci Eng* 46(11):11497–11518. <https://doi.org/10.1007/s13369-021-05949-1>
- Wen ZJ, Jiang PF, Jing SL et al (2021) Development and verification of simulation testing system for floor seepage in coal mine underground reservoir. *J China Coal Soc* 46(05):1487–1497. <https://doi.org/10.13225/j.cnki.jccs.st20.1601>
- Wu ZC (2017) Daliuta 22615 working face goaf overburden structure characteristics and surface subsidence prediction. Ph.D, Dissertation, Liaoning University of engineering and technology, Fuxin, China
- Yao QL, Hao Q, Chen XY et al (2019) Design on the width of coal pillar dam in coal mine underground reservoir. *J China Coal Soc* 44(03):891–899. <https://doi.org/10.13225/j.cnki.jccs.2018.6012>
- Zhang Y, Cao SG, Guo S et al (2018) Mechanisms of the development of water-conducting fracture zone in overlying strata during shortwall block backfill mining: a case study in Northwestern China. *Environ Earth Ence* 77:543. <https://doi.org/10.1007/s12665-018-7726-6>
- Zuo JP, Sun YJ, Qian MG (2017) Movement mechanism and analogous hyperbola model of overlying strata with thick alluvium. *J China Coal Soc* 42(06):1372–1379. <https://doi.org/10.13225/j.cnki.jccs.2016.1164>

Publisher's Note Springer Nature remains neutral with regard to jurisdictional claims in published maps and institutional affiliations.